

## The effect of ignition timing on engine performance in a laser ignition engine: A CFD study

Turan Alp Arslan<sup>1\*</sup>, Hüseyin Bayrakçeken<sup>1</sup>, Ahmet Altuncu<sup>2</sup>, Emin Çengelci<sup>3</sup>, Hamit Solmaz<sup>4</sup>

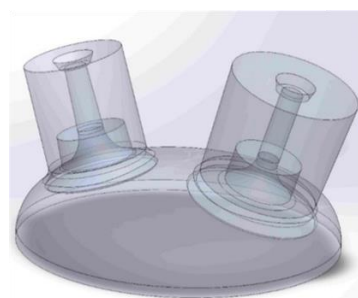
<sup>1</sup> Department of Automotive Engineering, Faculty of Technology, Afyon Kocatepe University, Afyonkarahisar 03200, Turkey

<sup>2</sup> Department of Electrical-Electronics Engineering, Faculty of Technology, Afyon Kocatepe University, Afyonkarahisar 03200, Turkey

<sup>3</sup> Department of Engine Vehicles and Transportation Technology, İsehisar Vocational School, Afyon Kocatepe University, Afyonkarahisar 03200, Turkey

<sup>4</sup> Department of Automotive Engineering, Faculty of Technology, Gazi University, Ankara 06500, Turkey

✉ [talparslan@aku.edu.tr](mailto:talparslan@aku.edu.tr)



### Highlights:

- Laser ignition systems offer advantages in enhancing engine performance, reducing fuel consumption, and lowering emissions compared to traditional spark ignition systems.
- Using ANSYS Fluent 2021 R1, the study found optimal engine performance at 680 °CA ignition timing with the laser ignition system, achieving 16.43 kW power, 62.76 Nm torque, and 61.56 bar peak pressure.
- The laser ignition system led to smoother, knock-free combustion, reduced in-cylinder temperatures, and shorter combustion durations, proving its potential in advancing engine and combustion performance.

### Abstract

As a result of the high-power output, low fuel consumption, and low emissions expected from internal combustion engines, new engine technologies continue to be developed. Laser ignition systems are a solution to these expectations with the advantages they offer. Experimental and numerical studies related to laser ignition systems are accelerating today. In this study, an internal combustion engine was simulated with the spark and laser ignition systems, and the changes in engine performance for different ignition timings were investigated comparatively. ANSYS Fluent 2021 R1 software was used in the dynamic CFD study in which the entire engine cycle was analysed. Analyses were carried out at constant engine speed with an iso-octane+air mixture. Critical parameters such as pressure, volume, and temperature changes, power, torque, IMEP, MPRR, peak pressure, HRR, CHRR, start of combustion, and combustion duration were evaluated for both ignition systems. As a result of the study, optimum performance values were obtained at 680 °CA ignition timing with laser ignition system. At this ignition timing, power, torque, IMEP, MPRR, and peak pressure values were determined as 16.4302 kW, 62.7635 Nm, 14.1743 bar, 2.4665 bar/°CA, and 61.5611 bar, respectively. The laser ignition system increased engine performance, and smoother and knock-free combustion occurred. At optimum ignition timing, combustion duration was shortened, and in-cylinder temperatures decreased. The findings show that the laser ignition system will contribute to engine development studies by positively affecting engine and combustion performance.

**Keywords:** CFD; Combustion analysis; Ignition timing; Laser ignition; Spark ignition

### Article info

Submitted:  
2024-10-11

Revised:  
2024-12-26

Accepted:  
2025-01-09



This work is licensed under  
 a Creative Commons  
 Attribution-NonCommercial 4.0  
 International License

### Publisher

Universitas Muhammadiyah  
 Magelang

## 1. Introduction

Today, developing technology, advances in the industry, the increasing population of countries, and growing economies cause an enhancement in the amount of energy used in transportation [1]–[3]. The fact that electric vehicles have problems such as battery-related

charging, safety, and range [4]–[8], which are still not fully resolved, makes it necessary to meet this increasing amount of energy with conventional fuels [9], [10]. Furthermore, despite the widespread use of electric vehicles, it is expected that internal combustion engines will continue to be used in generators, agricultural vehicles, rail vehicles, and sea vehicles for many years. However, conventional fuel sources cause greenhouse gas emissions, and limited fuel sources are rapidly depleted [11]. Due to the emerging energy scarcity and environmental problems, the limitations on exhaust emissions are increasing day by day, and fuel prices are increasing [12], [13]. Moreover, the competitive structure and customer requirements in the automotive industry increase the expectation of high power output [14]. This trend continues to challenge manufacturers and researchers to develop internal combustion engines. Meeting high power output, low fuel consumption, and demanding emission standards is possible by increasing thermal efficiency by using alternative fuels [15]–[17], alternative combustion modes [18]–[20], and new ignition technologies [21], [22]. This has led to the idea of developing laser ignition systems to improve combustion and engine performance, and it has become one of today's most important research topics for engines with different fuels such as methane [23], gasoline [24], hydrogen [25], diesel [26], and compressed natural gas [27].

Improving power and thermal efficiency in internal combustion engines is possible by increasing the charge density and compression ratio. The increased charge density increases the required spark energy, which requires a higher secondary coil voltage. The secondary coil voltage required for spark generation depends on the working gas pressure, temperature, and the distance between the spark plug electrodes. The voltage required for spark energy, which will provide efficient combustion at high charge density and compression ratio, causes erosion and deformation in the spark plug electrodes [28], [29]. In the laser ignition system, plasma is formed by concentrating the pulsed laser beam energy at a very small focal point. If the energy level is high enough, the fuel mixture in the cylinder ignites. Since there are no solid surfaces like electrodes in laser ignition, erosion, deformation, and heat loss from these surfaces do not occur [30]. This offers a great advantage for the life of the ignition system. Another focus of laser ignition is lean mixture combustion. Lean mixture combustion, which requires higher spark energy, improves thermal efficiency while reducing lost heat transfer, fuel consumption, exhaust emissions, and knock [31]. However, the prolongation of the flame propagation distance becomes a problem, especially in lean mixture engines with large cylinder diameters. Flame velocity can be increased by turbulent movements or by shortening the flame propagation distance in lean mixture engines [32], [33]. It is possible to shorten the flame propagation distance by using more than one spark plug in a cylinder or by determining the optimum position of the ignition start in the combustion chamber [34], [35]. The use of more than one spark plug for each cylinder increases the number of equipment and costs, and makes the design, assembly, and maintenance processes more troublesome. Due to the placement of the spark plug in the cylinder head, the spark is formed at a point very close to the top of the combustion chamber. For this reason, it is difficult to obtain the optimum position for ignition start [28]. With laser ignition, high-energy ignition is created at multiple points in the combustion chamber, thus shortening the combustion duration in lean mixtures [36]. The ignition position can be optimized by changing the focal length of the lens in the system. With laser ignition, more precise control over ignition timing, spark position, and spark energy can be achieved, while ignition delay time is reduced [37], [38]. In addition to all these advantages, the laser ignition system has disadvantages such as low laser stability, negative effects of combustion residues on optical systems, operating difficulties due to temperature and vibration, a large area of the integrated system, high cost, and application difficulties [39]–[41]. The advantages of the system offer great potential for wide application areas of internal combustion engines. However, due to its disadvantages, it is still very difficult to provide a completely effective and safe laser ignition [23]. In order to benefit from the existing potential and eliminate the disadvantages, the interest in laser ignition and the number of studies on this subject are increasing day by day [42]–[45].

When the past studies are examined, it is seen that the internal combustion engine and laser ignition system are exposed to challenging conditions such as high temperature, pressure, and vibration. Configuration changes on the engine and ignition system result in high costs and long installation times. As an alternative to experimental studies, the use of advanced CFD codes in internal combustion engines can be presented. With the CFD method, repeatable simulations can be performed with a large number of configurations and different boundary conditions [46], [47]. While the data obtained in experiments are generally limited to temperature and pressure measurements at determined points, in simulations flow fields, pressure, and temperature

distributions can be obtained. With a simulation in which appropriate method and boundary conditions are defined, mixture preparation, injection, ignition and combustion processes can be examined, and related subsystem and geometry optimizations can be performed [48]. The simulation method saves cost and time, as well as provides highly accurate results [49]. Commercial software such as ANSYS Fluent, CONVERGE, KIVA, STAR-CD, COMSOL, VECTIS or FORTRAN, MATLAB and C-based personal codes are widely used for internal combustion engine simulations [50]–[52]. Numerical studies on the development of laser-ignition engines have also accelerated in recent years. As in experimental studies, it is seen that numerical studies are generally carried out under constant volume conditions with different fuels such as hydrogen [53], methane [54] and gasoline [55] or without fuel [56].

When the experimental and numerical studies related to laser ignition are examined, it is seen that few studies have been done with the iso-octane+air mixture as fuel. The number of studies examining the effects of ignition timing for laser ignition is also very limited. In addition, numerical studies were mostly carried out at constant volume, and no numerical study with a dynamic structure covering the entire engine cycle was found. In this study, an internal combustion engine model was created, and the effects of spark and laser ignition on engine and combustion performance were investigated numerically for different ignition timings. In-cylinder pressure and temperature data obtained from the analysis results were converted into engine and combustion performance parameters with appropriate equations. The advantages of the laser ignition system on critical parameters such as pressure, volume and temperature changes, power, torque, IMEP, MPRR, peak pressure, HRR, CHRR, start of combustion, and combustion duration are discussed.

## 2. Literature Review

In recent years, there have been many studies on using laser ignition systems in internal combustion engines to improve engine performance and reduce fuel consumption and exhaust emissions. These experimental and numerical studies aim to overcome the disadvantages of laser ignition systems, such as design and application difficulties, high cost, and large space occupied. These studies mainly focus on reducing the ignition energy, determining the optimum focal point, and determining the appropriate fuel type and mixture ratio for laser ignition. In the coming days, with the developments in optical systems and internal combustion engine technology, it is expected that these problems will be solved and laser ignition systems will be commonly used.

Kumar and Agarwal compared the performance of a spark ignition system and a laser ignition system in a constant-volume combustion chamber. The experiments were carried out at 4 bar and 150 °C with three hydrogen-enriched natural gas mixtures and three air-fuel mixture ratios ( $\lambda$ : 1.0, 1.2, and 1.4). The laser ignition system used three different lens combinations and two different focal points. The laser ignition system showed superior combustion characteristics, especially a significantly reduced combustion duration. Similarly, the hydrogen enrichment ratio reduced the peak pressure value and shortened the combustion duration. As a result of the study, it was reported that the ability to select the central position with laser ignition is advantageous for combustion performance, providing faster combustion, higher engine power, and lower specific fuel consumption compared to spark ignition [57].

Agarwal et al. investigated the effect of laser ignition system parameters (laser pulse energy and ignition timing) on particulate emissions in hydrogen-powered internal combustion engines. The experimental study used a hydrogen-powered engine with different compression ratios. During the experiments, particle concentration increased with increasing engine load, nucleation mode particle (NMP), and accumulation mode particle (AMP) increased with increasing laser pulse energy. Similarly, particle concentration increased with increasing ignition timing and higher compression ratio. The study proved that particle emissions could be effectively controlled by optimizing laser parameters and compression ratio in hydrogen-fuelled engines [58].

Azarmanesh and Targhi performed methane-air mixture combustion in an internal combustion engine with a laser ignition system. The results showed that laser ignition shortened the combustion duration for different equivalence ratios than spark ignition. At a 0.7 equivalence ratio, the laser ignition system improved thermal efficiency by 8.13%, average pressure by 10%, specific fuel consumption by 27.44%, and maximum pressure by 37.83% compared to the spark ignition system. At 0.6 equivalence ratio, complete combustion could not be achieved using spark plugs, and this problem was solved with laser ignition. As a result of the study, it was stated that the laser ignition system could provide solutions to issues such as low flame speed, imperfect combustion, and lean combustion limit improvement [59].

Pavel et al. operated a petrol passenger car with multipoint fuel injection using a laser ignition system. The internal combustion engine was tested at a speed of 2000 rpm and constant load conditions with a brake mean effective pressure of 2 bar and different ignition timings. As a result of the experiments carried out with stoichiometric ( $\lambda: 1$ ) and lean mixture ( $\lambda: 1.25$ ), engine performance and exhaust emissions were analyzed comparatively with the spark ignition system. The laser ignition system increased engine brake power by 7.9% under stoichiometric conditions and 29% under lean mixture conditions. Specific fuel consumption decreased by 7.4% in stoichiometric and 21% in lean mixture conditions with the laser ignition system. Using the laser ignition system, CO emissions were reduced by approximately 30%, and THC emissions decreased by approximately 6%. NOx emissions increased significantly with the use of laser ignition. As a result of the study, it was emphasized that using laser ignition systems in internal combustion engines could provide advantages in leaner mixtures, higher loads, and high engine speeds. In addition, the laser ignition system is predicted to be reliable and cost-competitive with the developing technology [24].

Patil and Nandgaonkar numerically modeled the ignition of a gasoline-air mixture in a constant-volume combustion chamber using a laser ignition system. ANSYS Fluent 17.2 software was used to analyze the peak pressure and emission values depending on the varying equivalence ratio ( $\lambda: 0.8-1.4$ ). Under rich mixture conditions ( $\lambda: 1.4$ ), the peak pressure value was measured as 0.67 MPa with an error of 3.43%, and the combustion duration under stoichiometry conditions was measured as 31.5 ms with an error of 1.61%. CO emissions increased significantly with the enrichment of the mixture, while NOx and CO<sub>2</sub> emissions decreased. As a result of the study, it was stated that laser ignition could work successfully under rich mixture conditions and replace spark ignition for liquid fuels in the future [55].

Do et al. numerically compared laser and spark plug ignition systems on a 125 cc motorcycle engine. The simulation model created with ANSYS Fluent software analyzed parameters such as air mass into the cylinder, ignition energy, engine power and torque, and specific fuel consumption. In the engine model using a laser ignition system, positive results were obtained in volumetric efficiency, power, torque, emission, and fuel consumption. The laser ignition system had no significant effect at low engine speeds [60].

Bhondwe and Koshti numerically modeled a laser ignition system for the ignition of methane-air mixture in a constant volume combustion chamber. In the study carried out using STAR CCM+ software, the Nd-YAG 1064 nm laser system was simulated, and the time-dependent variations of pressure and mass fractions were investigated. As a result of the study, it was determined that the lean methane-air mixture caused a longer combustion duration [61].

### 3. CFD Modeling Approach

ANSYS Fluent 2021 R1 software was used in this study, in which the effects of spark and laser ignition in an internal combustion engine on combustion and engine performance at different ignition timings were investigated numerically. The working process in which the CFD method is used mainly consists of four stages. In the first stage, a physical model was created by determining the detailed features and dimensions of the analysis engine. Piston and valve movements are added to the model for the solution of a dynamic and realistic combustion analysis that changes depending on time. Afterward, the modeling phase was completed by determining the basic parameters of the spark and laser ignition. In the second stage, a dynamic mesh structure suitable for the solution of the problem was created, the control of the mesh structure was ensured, and appropriate solution methods were determined. In the third stage, the boundary conditions and fuel properties were defined by the software, and the solution of the combustion analysis was carried out. In the last stage of the study, the obtained analysis results were transferred to a specially created calculation sheet, where they were converted into parameters related to combustion and engine performance and evaluated.

The materials and methods used in this research are described in detail below in five sections: governing equations, analysis engine model and properties, meshing strategy and analysis methods, boundary conditions and fuel properties, and evaluation of analysis results.

#### 3.1. Governing Equations

As in other numerical methods, CFD applications also create a mathematical model with equation sets consisting of partial differential equations, integral equations, and boundary conditions. These equations, which form the basic building blocks of numerical studies, are called

governing equations [62], [63]. In CFD applications, the solution region is divided into finite elements, and the flow and heat movements are solved by these governing equations.

The general expression of the conservation of mass equation valid for both compressible and incompressible flows is as in Eq. (1).

$$\frac{\partial \rho}{\partial t} + \nabla(\rho v) = 0 \quad (1)$$

The left side of the conservation of momentum equation in Eq. (2) includes the mass and acceleration components, and the right side contains the force components. Force components consist of external forces such as gravity, pressure gradients, and internal stress forces [64].

$$\rho \left( \frac{\partial v}{\partial t} + v(\nabla v) \right) = -\nabla P + \nabla \tau + \rho g \quad (2)$$

The conservation of energy equation is seen in Eq. (3). The terms to the right of the equation represent, conduction, species diffusion, viscous energy transfer, and chemical reaction heat, respectively [64].

$$\frac{\partial}{\partial t}(\rho E) + \nabla(v(\rho E + P)) = \nabla \left( k_{eff} \nabla T - \sum_j h_j J_j + (\tau_{eff} v) \right) + S_h \quad (3)$$

The standard k-ε turbulence model is a quasi-experimental model consisting of the transfer equations of turbulent kinetic energy and its dispersion ratio. In this model, it is assumed that the molecular viscosity effects are negligible and the flow is completely turbulent. Turbulence kinetic energy and dispersion ratio are obtained by the transfer equations seen in Eq. (4) and Eq. (5) [62].

$$\frac{\partial}{\partial t}(\rho k) + \frac{\partial}{\partial x_i}(\rho k v_i) = \frac{\partial}{\partial x_i} \left[ \left( \mu + \frac{\mu_t}{\sigma_k} \right) \frac{\partial k}{\partial x_j} \right] + G_k + G_b - \rho \varepsilon - Y_M + S_k \quad (4)$$

$$\frac{\partial}{\partial t}(\rho \varepsilon) + \frac{\partial}{\partial x_i}(\rho \varepsilon v_i) = \frac{\partial}{\partial x_i} \left[ \left( \mu + \frac{\mu_t}{\sigma_\varepsilon} \right) \frac{\partial \varepsilon}{\partial x_j} \right] + G_{1\varepsilon} \frac{\varepsilon}{k} (G_k + C_{3\varepsilon} G_b) - G_{2\varepsilon} \rho \frac{\varepsilon^2}{k} + S_\varepsilon \quad (5)$$

Multiple and simultaneous chemical reactions can be modeled volumetrically or by reactions occurring on wall surfaces. In the combustion analysis, the species transport equation seen in Eq. (6) is used because of the transport of different types of chemicals and their volumetric reaction in the combustion chamber.

$$\frac{\partial}{\partial t}(\rho Y_i) + \nabla(\rho v Y_i) = -\nabla J_i + R_i + S_i \quad (6)$$

$$R_{i,r} = v'_{i,r} M_{w,i} A \rho \frac{\varepsilon}{k} \min_R \left( \frac{Y_R}{v'_{r,r} M_{w,R}} \right) \quad (7)$$

$$R_{i,r} = v'_{i,r} M_{w,i} A B \rho \frac{\varepsilon}{k} \frac{\sum_P Y_P}{\sum_j^N v'_{j,r} M_{w,j}} \quad (8)$$

### 3.2. Analysis Engine Model and Specifications

A single cylinder, four-stroke, naturally aspirated, two-valve, and spark-ignition internal combustion engine model was used in the study in which combustion with the spark and laser ignition was analysed. The combustion chamber of this engine is hemispherical, the piston crown is flat, and the intake and exhaust ports are angled. Fuel injection to the engine takes place through the intake port. The basic features of the modeled engine are shown in Table 1. The engine speed was set to 2500 rpm for all analyses. The opening-closing times of the intake and exhaust valves and the lift amounts are defined to the Fluent software with a profile file. Valve overlap is 56 °CA. In the analysis setup, stroke volume and compression ratio values were determined by using crank radius, connecting rod length, and engine speed. Based on these values, the piston position, and volume changes were calculated.

**Table 1.**  
Engine specifications

| Engine Parameters                       | Specifications                   |
|---|----------------------------------|
| Engine type                             | Single cylinder, four stroke, SI |
| Fuel type                               | Gasoline                         |
| Engine speed (rpm)                      | 2500                             |
| Fuel injection                          | Port fuel injection              |
| Valve per cylinder                      | 2                                |
| Bore (mm) x Stroke (mm)                 | 84 x 100.4                       |
| Crank radius (mm)                       | 50.2                             |
| Connecting rod length (mm)              | 200.8                            |
| Clearance volume (cm <sup>3</sup> )     | 80.9                             |
| Swept volume (cm <sup>3</sup> )         | 556.4                            |
| Total volume (cm <sup>3</sup> )         | 637.3                            |
| Compression ratio                       | 7.88 : 1                         |
| Intake valve opening and closing (°CA)  | 332 and 606                      |
| Exhaust valve opening and closing (°CA) | 112 and 388                      |
| Maximum valve lifts (mm)                | 9.525                            |

In the analyses carried out, spark and laser ignition methods were used and their effects on combustion and engine performance were investigated. The analyses were repeated with two different ignition methods by changing the ignition timing at 5° intervals from 680 °CA to 700 °CA. The flame starting point is in the middle of the hemispherical combustion chamber and at a depth of 12 mm from the top. This amount of depth equals the laser focal length. Since the effect of a spark plug ground electrode geometry of this length on the in-cylinder flow dynamics is very small and negligible, a single flow volume design was used for both engine geometries. The parameters of both ignition systems are shown in [Table 2](#).

**Table 2.**  
Ignition specifications

| Ignition Parameters   | Spark Ignition         | Laser Ignition          |
|-----------------------|------------------------|-------------------------|
| Ignition timing (°CA) | 680→700                |                         |
| Duration (s)          | 1 x 10 <sup>-3</sup>   | 1 x 10 <sup>-8</sup>    |
| Energy (J)            | 0.1                    |                         |
| Initial radius (m)    | 2.5 x 10 <sup>-4</sup> | 8.11 x 10 <sup>-6</sup> |

**Table 3.**  
Laser parameters

| Laser Parameters             | Values |
|------------------------------|--------|
| Beam diameter (mm)           | 2      |
| Laser beam quality parameter | 1      |
| Wavelength (nm)              | 1064   |
| Focal length (mm)            | 12     |

The physical properties of the spark plug and the laser beam were determined in accordance with the experimental and numerical studies performed on similar engine types [65]–[70]. The laser beam parameters selected in accordance with the designed internal combustion engine model are shown in [Table 3](#). Using these parameters and Eq. (9), the laser spot size is calculated.

$$S = \frac{4M^2 \lambda f}{\pi d} \quad (9)$$

### 3.3. Meshing Strategy and Analysis Methods

The dynamic mesh structure is used to solve the numerical problem in which the flow volume changes depending on time is modeled. With the dynamic mesh structure, all times of an engine cycle can be analyzed precisely and in detail. This method allows the flow volume to be updated at each time step depending on the defined equations of motion. Thus, the volume and pressure changes due to piston and valves movements during the cycle can be simulated the closest way to real conditions. For this reason, it is essential to use a dynamic mesh structure to analyze the entire cycle of an internal combustion engine in detail.

In the combustion simulation setup performed in Fluent software, the mesh production was completed in four stages. In the first stage, the mesh type and basic mesh properties were determined with the ANSYS Mesh module. While the selected polyhedral mesh type yields results very close to other element types, such as tetrahedral and hexahedral, it can achieve much faster solution times by reducing the number of elements by half [71]. This feature of the mesh type also means faster convergence with fewer iterations. In the second stage, dynamic mesh structure details are defined in Fluent software. Smoothing, layering, and remeshing methods were used as dynamic mesh generation methods. Then, the parts and regions of the engine were defined, and the inlet, outlet, and internal flow environments were determined. In this step of creating a dynamic mesh structure, the intake and exhaust valve lifts, which change depending on the crank angle, are transferred to the software with a profile file (.prof). The mesh structure movements seen on the piston and cylinder wall were created with the engine speed, crank radius, and

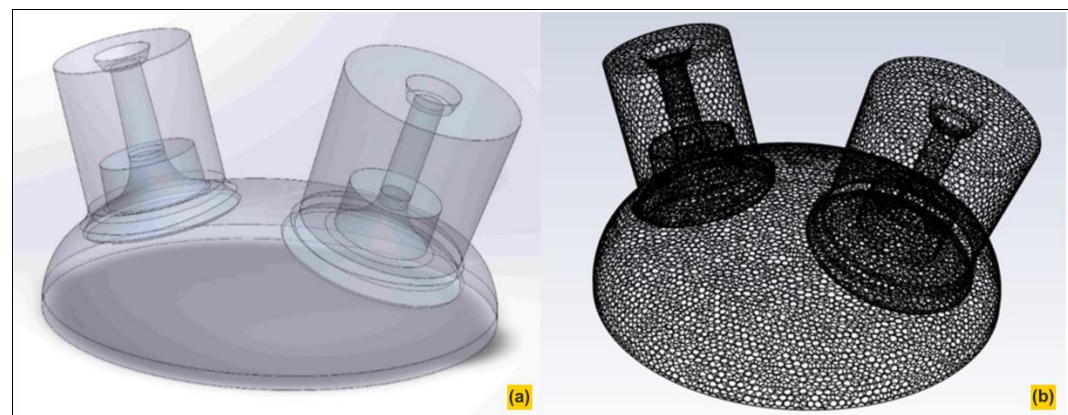
connecting rod length values defined in the IC Engine module. The mesh details of the engine model are shown in Table 4.

**Table 4.**  
Mesh details

| Mesh Parameters                            | Specifications                 |
|--|--------------------------------|
| Mesh type                                  | Dynamic mesh                   |
| Element type                               | Polyhedral                     |
| Number of elements                         | 61156                          |
| Number of nodes                            | 310849                         |
| Dynamic mesh methods                       | Smoothing, Layering, Remeshing |
| Smoothing methods                          | Spring/Laplace/Boundary layer  |
| Spring constant factor for smoothing       | 0.9                            |
| Convergence tolerance factor for smoothing | 0.001                          |
| Maximum number of iterations for smoothing | 20                             |
| Layering methods                           | Ratio based                    |
| Split factor for layering                  | 0.4                            |
| Collapse factor for layering               | 0.4                            |
| Remeshing methods                          | Local cell, region face        |
| Maximum length scale for remeshing (m)     | 0.0012                         |
| Maximum cell skewness for remeshing        | 0.7                            |

After defining the basic mesh properties, dynamic mesh settings, and wall motions, the mesh structure was examined throughout the entire engine cycle, and quality parameters were controlled in the final stage. By using hemispherical combustion chamber and flat piston design in the analysis engine, uniform distribution of the mesh structure has been achieved. A detailed design that includes cavities and bumps to be created in the piston crown and cylinder head increases the number of mesh elements and the number of nodes. In addition, elements with different sizes and properties directly affect the mesh quality parameters aspect ratio and orthogonality values. With the engine design used, it is aimed to reduce the solution time and improve the mesh quality. The flow volumes and mesh structure of the engine model at 0 °CA, where the piston is at the TDC, are shown in Figure 1.

**Figure 1.**  
Analysis engine:  
(a) Flow volume;  
(b) Mesh structure



The acceptable limits of orthogonality and aspect ratio values, which are indicators of the mesh structure quality, and the quality parameters of the laser ignition analysis engine are shown in Table 5. The fact that these values are in the ranges recommended in the literature confirms the suitability of the mesh structure [72]. In cases where mesh quality parameters are inappropriate, element type, number of elements, and other detailed mesh settings should be reconfigured, and quality parameters should be reviewed. The mesh structure, optimized in accordance with the quality parameters and grid independence study, has 61156 element numbers and 310849 nodes for 0 °CA where the piston is at TDC.

**Table 5.**  
Mesh quality parameters

| Quality Parameters    | Values  | Recommended | Adequacy |
|-----------------------|---------|-------------|----------|
| Maximum aspect ratio  | 5.16916 | < 40        | Good     |
| Minimum orthogonality | 0.46499 | > 0.2       | Good     |

For the time dependent dynamic analysis of the internal combustion engine, the pressure-based solver and the coupled solution method are used, which offer some advantages in terms of the accuracy of the solution results and the convergence speed of the solution compared to other

methods [72]. The pressure-based solver is capable of stable solutions in compressible flow conditions with high velocities. The coupled algorithm offers an efficient single-phase application for steady-state streams, with superior performance compared to other methods using the predict-fix approach [62]. Although many different views have been put forward in the modeling of turbulent flows, the k-ε turbulence model is widely used in CFD applications of internal and external combustion engines with its practicality and realistic approaches [73]–[76]. In combustion analysis, volumetric reaction and species transport models were preferred, since different types of chemicals are transported and reacted on a volumetric basis in the combustion chamber. The Finite

**Table 6.**  
Analysis methods

| Analysis Parameters               | Specifications               |
|-----------------------------------|------------------------------|
| Solver type                       | Pressure based               |
| Time                              | Transient                    |
| Pressure-velocity coupling        | Coupled                      |
| Species model                     | Species transport            |
| Reactions                         | Volumetric                   |
| Turbulence-chemistry interactions | Finite rate/Eddy dissipation |
| Viscous model                     | Standart k-ε                 |
| Number of time steps              | 720                          |
| Maximum iterations/Time step      | 20                           |
| Time step size (s)                | 6.66667 x 10 <sup>-5</sup>   |

rate/Eddy dissipation reaction model, which is used in combustions with relatively low turbulence-chemical and slow chemical interactions, in which reaction rates are controlled by turbulence, was chosen. The analysis methods used in the study are shown in **Table 6.**

### 3.4. Boundary Conditions and Fuel Properties

The boundary conditions of the combustion analysis carried out in a single-cylinder internal combustion engine are shown in **Table 7.** The engine geometry is divided into five different regions: the cylinder head, the cylinder wall, the intake region, the exhaust region, and the piston crown, and the surface temperatures suitable for an engine that has reached its operating regime are assigned to these regions. Relevant literature studies were utilized to choose the engine parts' temperature values [77]–[79]. The boundary conditions were determined by considering the reference values taken from these studies and the real operating conditions of an engine. The fuel mixture is intake into the cylinder under standard conditions. The combustion temperature primarily affects the piston crown, cylinder head, and cylinder walls. In real conditions, the cylinder head and cylinder walls are cooler than the piston crown because they are cooled by cooling water. Since the residual gases from combustion are discharged through the exhaust, these parts are dire-

**Table 7.**  
Boundary conditions

| Boundary Conditions            | Values               |
|--------------------------------|----------------------|
| Inlet pressure                 | Atmospheric pressure |
| Exhaust pressure               | Atmospheric pressure |
| Cylinder head temperature (K)  | 400                  |
| Cylinder wall temperature (K)  | 400                  |
| Inlet temperature (K)          | 298                  |
| Intake region temperature (K)  | 350                  |
| Exhaust region temperature (K) | 550                  |
| Piston temperature (K)         | 500                  |

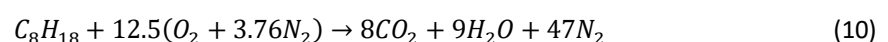
ctly exposed to high temperatures. The relatively cold mixture from the intake valves cools the intake area regularly. Since the analysis engine is naturally aspirated, the intake and exhaust pressures equal atmospheric pressure.

The octane number is an indicator of the knock resistance of gasoline. Iso-octane is a knock-resistant fuel, and its octane number is assumed to be 100. Iso-octane fuel is used as a reference fuel in experimental and numerical combustion analyses. In all combustion analyses in this study,

**Table 8.**  
Fuel properties

| Fuel Properties                              | Values         |
|--|----------------|
| Fuel Type                                    | iso-octane+air |
| Equivalence ratio                            | 1              |
| C <sub>8</sub> H <sub>18</sub> mole fraction | 0.016528925    |
| O <sub>2</sub> mole fraction                 | 0.20661157     |
| N <sub>2</sub> mole fraction                 | 0.776859505    |

iso-octane+air mixture in stoichiometric ratio was used as the standard fuel. The properties of the fuel mixture used are shown in **Table 8,** and the combustion equation is shown in Eq. (10).



Where, C<sub>8</sub>H<sub>18</sub> is the iso-octane, O<sub>2</sub> is the oxygen, N<sub>2</sub> is the nitrogen, CO<sub>2</sub> is the carbon dioxide, and H<sub>2</sub>O is the water.

### 3.5. Evaluation of Analysis Results

In order to evaluate the results of the analysis whose solution was completed, in-cylinder pressure and temperature values were recorded throughout the entire engine cycle depending on

time. The recorded values were transferred to a specially designed calculation sheet and converted into engine performance values with the equations defined here. First of all, the crank angle at the current time, the piston position relative to the BDC, and the volume values were determined by using the time step and the dimensional properties of the engine. Then, in-cylinder pressure and temperature values were included in these calculations. With the defined equations, critical parameters such as work, power, torque, IMEP, MPRR, peak pressure, HRR, CHRR, start of combustion, end of combustion, and combustion duration were obtained. All these parameters, which are widely used in both experimental and numerical studies, are of great significance in the evaluation of engine and combustion performance. The net amount of work produced during the cycle in the analysis engine is calculated by Eq. (11) [80].

$$W_i = \oint P dV \quad (11)$$

IMEP is defined as the average pressure acting on the piston during the cycle and is calculated by Eq. (12) [81].

$$IMEP = \frac{W_i}{V_{sw}} = \frac{P_i i}{V_{sw} n} \quad (12)$$

Indicated power and torque values are proportional to net work and engine speed and are calculated by Eq. (13) and Eq. (14), respectively.

$$P_i = \frac{W_i n}{i} \quad (13)$$

$$T_i = \frac{P_i}{n 2\pi} \quad (14)$$

HRR is calculated by Eq. (15) according to the first law of thermodynamics [82]. CHRR, which is an important parameter in the evaluation of the efficiency of the combustion process, is obtained by integrating the HRR values calculated based on the crank angle change. CHRR is shown by Eq. (16) [83].

$$\frac{dQ}{d\theta} = \frac{1}{k-1} V \frac{dP}{d\theta} + \frac{k}{k-1} P \frac{dV}{d\theta} \quad (15)$$

$$Q_c = \int \frac{dQ}{d\theta} \quad (16)$$

In the combustion analysis, an iso-octane+air mixture is used as fuel. The specific heat ratio of the mixture used in the calculation of HRR is determined by Eq. (17) and Eq. (18) according to the mass ratios of the components.

$$k = \frac{C_{p,mix}}{C_{v,mix}} \quad (17)$$

$$C_{p,v,mix} = \left( \frac{m_1}{m_{mix}} \right) C_{p,v1} + \left( \frac{m_2}{m_{mix}} \right) C_{p,v2} \quad (18)$$

The CA10 and CA90 values indicate the position of the CHRR, in terms of crank angle, which has reached 10% and 90% of its maximum value, respectively [84]. Among these values, which are frequently used in the analysis of combustion duration, CA10 represents the start of combustion, and CA90 represents the end of combustion.

MPRR is the maximum value of the in-cylinder pressure change depending on the crank angle change and is calculated by Eq. (19). Peak pressure is the maximum amount of in-cylinder pressure reached throughout the cycle.

$$MPRR = \left[ \frac{dP}{d\theta} \right]_{max} \quad (19)$$

## 4. Results and Discussions

In this study, the effect of spark and laser ignition systems on engine performance in an internal combustion engine was investigated numerically for different ignition timings. The power, torque, IMEP, MPRR, peak pressure, start of combustion, and combustion duration values, which are critical for engine and combustion performance, were compared for both ignition systems. Pressure, temperature, HRR, and CHRR diagrams of the analysis engine with laser ignition system were examined for all ignition timings. The results obtained at the end of the research are explained in detail in the following sub-sections.

### 4.1. In-cylinder Pressure and Temperature Contours

The pressure and temperature contours obtained in the analyzed engine using laser ignition are illustrated in Figure 2. The pressure and temperature contours are obtained for 700 °CA ignition timing. Analysis results in the longitudinal cross-sectional view of the engine model presented at 90 °CA intervals to include all strokes of an engine cycle. When the figure is examined, it is seen that the intake, compression, power, and exhaust strokes are simulated in accordance with the real conditions.

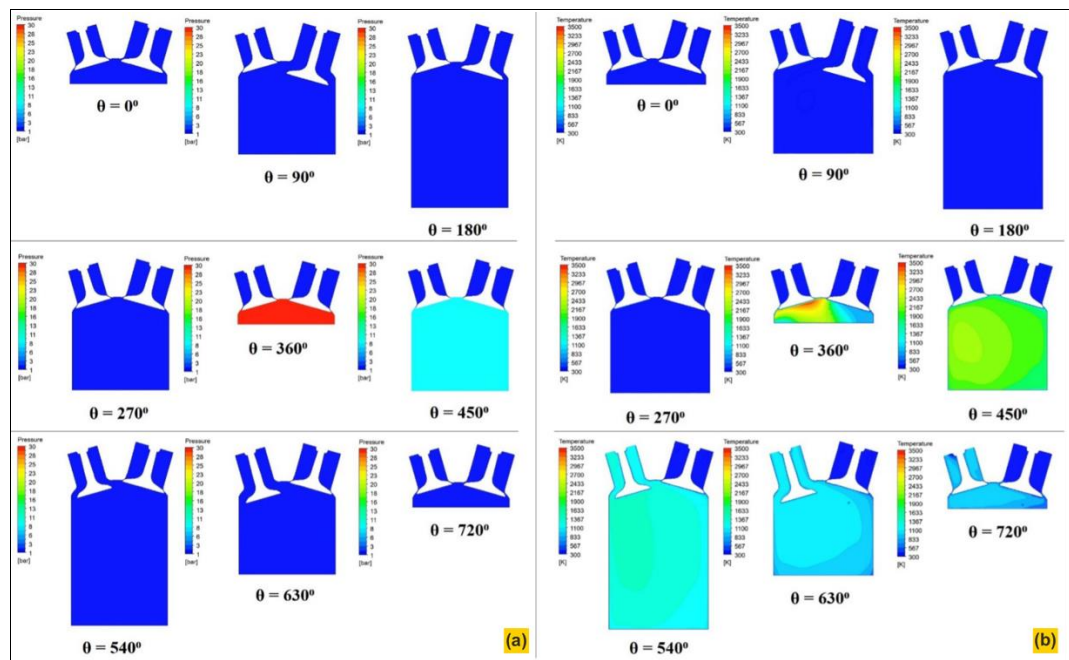


**Figure 2.** Dynamic analysis results for 700 °CA laser ignition timing: (a) Pressure contours; (b) Temperature contours

### 4.2. Power and Torque

Higher power and torque values were obtained for all ignition timings from the analysis engine in which laser ignition was used. The variation of power and torque values depending on the ignition timing is shown in Figure 3. The optimum ignition timing was determined as 680 °CA for both ignition systems, under these analysis and operating conditions. At this ignition timing, 16.4302 kW power and 62.7635 Nm torque were obtained from the laser ignition analysis engine.

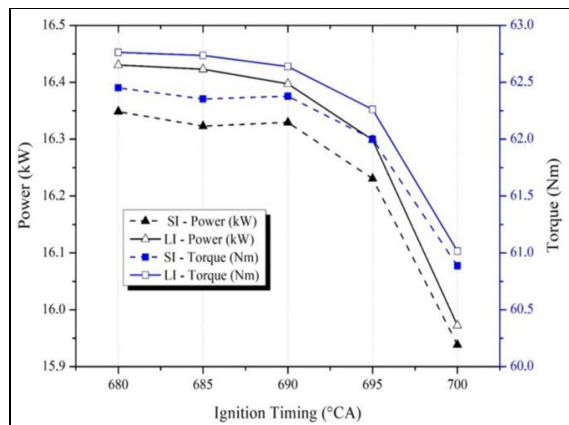


**Figure 3.** Variation of power and torque with ignition timing

The power and torque values obtained from the spark ignition engine under the same conditions are 16.3485 kW and 62.4515 Nm, respectively. Both laser and spark ignition engines showed a rapid decrease in power and torque after ignition timing of 690 °CA. Maximum pressure build-up after this ignition timing occurs well after TDC. With delayed ignition, more fuel burned during expansion time, causing a decrease in in-cylinder pressure and temperature. It is seen that varying ignition timing has a similar effect on both ignition

systems. With the appropriate ignition timing, the maximum pressure is created soon after the TDC, so that the power and torque values reach the maximum level.

### 4.3. IMEP, MPRR and Peak Pressure

The variation of IMEP, MPRR, and peak pressure values depending on the ignition timing is shown in Figure 4. As in the power and torque values, better performance was obtained for these

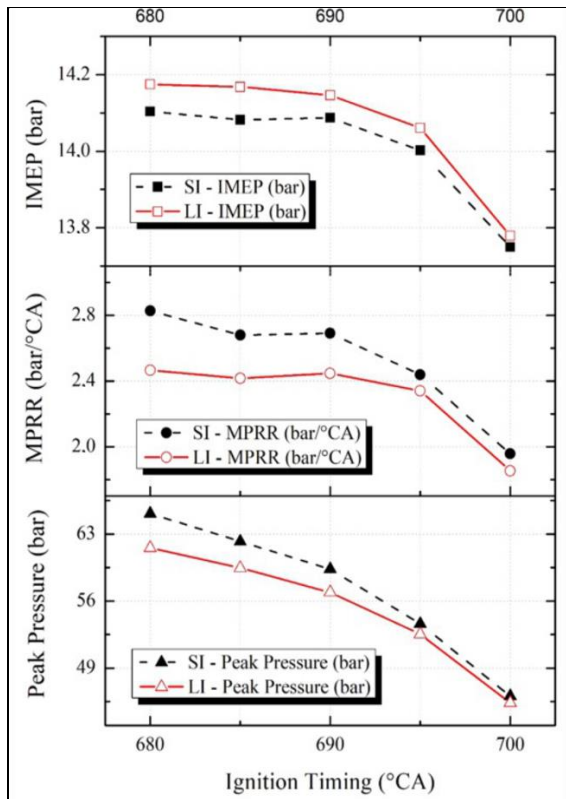


Figure 4. Variation of IMEP, MPRR, and peak pressure with ignition timing

parameters with a laser ignition system. At the optimum ignition timing of 680 °CA, the IMEP, MPRR, and peak pressure values for the laser ignition engine were 14.1743 bar, 2.4665 bar/°CA, and 61.5611 bar, respectively. In the spark ignition engine, these parameters were 14.1038 bar, 2.8279 bar/°CA, and 65.1447 bar. The IMEP value, which expresses the average of the pressures acting on the piston during a cycle and has an important place among the engine performance parameters, took a higher value with a small difference in laser ignition and showed a rapid decrease with the decreasing ignition advance. Due to the smooth burning characteristic, which is one of the important features of laser ignition, MPRR and peak pressure amount were higher in spark ignition. This situation will directly affect the probability of knocking and the amount of knocking, and will ensure that the laser ignition engine operates more noiselessly, vibration-free, and durable at higher power output [85], [86].

### 4.4. Start of Combustion and Combustion Duration

The variation of the start of combustion and combustion duration depending on ignition timing is presented in Figure 5. In the evaluation of the analysis results, the crank angle from which CA10 value is obtained is considered as the start of combustion, the crank angle from which the CA90 value is obtained as the end of combustion, and the crank angle between the start of combustion and the end of combustion is considered as the combustion duration. At 680 °CA ignition timing, the combustion duration is 26.997 °CA for the laser ignition engine and 27.14 °CA for the spark ignition engine. At 685 °CA ignition timing, the combustion durations are 25.132 °CA and 26.328 °CA for laser and spark ignition engines, respectively. It has been determined that the combustion duration is shorter in the laser ignition engine at 680 and 685 °CA ignition timing. The

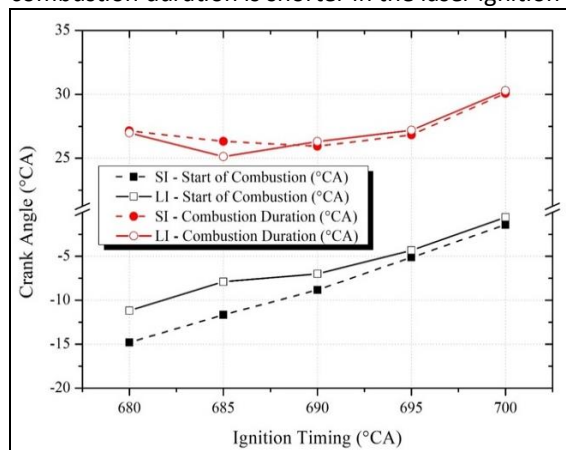


Figure 5. Variation of start of combustion and combustion duration with ignition timing

shortening of the combustion duration in these ignition timings will increase the NOx emissions and decrease the THC and CO emissions [87]. It is seen that the combustion duration is shorter in the spark ignition analysis engine with decreasing ignition advance values. However, in these ignition advances, the engine power is already less for spark ignition and decreases rapidly for both ignition systems. For all ignition timings, combustion starts at later crank angles in the laser ignition system. This can be attributed to the small initial spark radius of laser ignition.

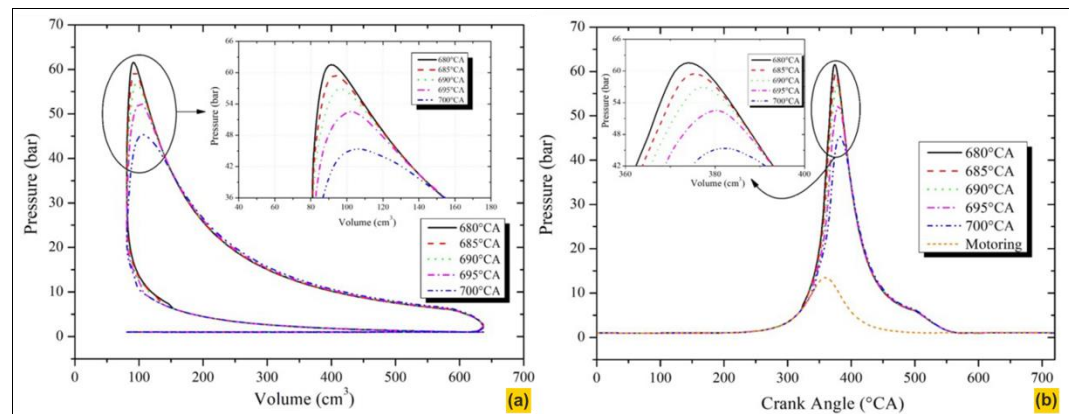
When the studies in the literature are examined, it is seen that laser and spark ignition offer very close results in terms of engine and combustion performance parameters. However, the laser

ignition system is superior to the spark ignition system in all varying ignition timings because of its high accuracy and stable operation capability. Lower MPRR and maximum in-cylinder pressure reduce the possibility and amount of knocking. Low in-cylinder temperatures and low combustion duration have a favorable effect on emissions and combustion efficiency. Especially with the smoother combustion provided by the laser ignition system, THC, NO<sub>x</sub>, and CO emissions and specific fuel consumption are reduced. Similar results on all these critical parameters have been obtained in numerical and experimental studies in the literature and support the results of the analyses performed in this study [24], [28], [29], [88], [89].

#### 4.5. In-cylinder Pressure

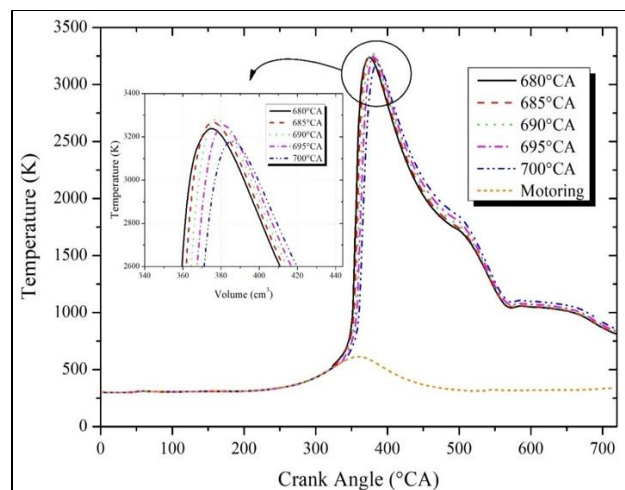
The pressure-volume diagrams obtained at different ignition timings of the laser ignition analysis engine are shown in **Figure 6a**, and the pressure-crank angle diagrams are shown in **Figure 6b**. The pressure increase and decrease forms in the diagrams are very similar to the results obtained from a real test engine. The increased ignition advance amount creates a pressure increase in the combustion region of the diagram directly. This is due to the emergence of the maximum amount of pressure in the cylinder at the appropriate time. Similar to other performance results, the net work rate and in-cylinder peak pressure increased at the optimum ignition timing of 680 °CA. In internal combustion engines, the high-pressure gases generated by combustion push the piston downwards and transfer mechanical energy to the crankshaft, and this process is defined as positive work. For this process to take place efficiently, it is critical that the ignition advance, i.e., the fuel-air mixture's ignition timing, is adjusted according to the crankshaft position. If the ignition advance is not set correctly, combustion can be delayed or occur prematurely, adversely affecting the amount of positive work and the engine's efficiency. In the optimum ignition advance, after the piston exceeds soon after the TDC, the maximum pressure emerges, and the amount of positive work increases. With the reduction of the ignition advance, the time interval in which the maximum pressure emerges passes into the expansion stroke, and as a result, the amount of positive work on the piston decreases.

**Figure 6.**  
(a) Pressure-volume diagrams for laser ignition timings;  
(b) Pressure-crank angle diagrams for laser ignition timings



#### 4.6. In-cylinder Temperature

**Figure 7.**  
Temperature-crank angle diagrams for laser ignition timings



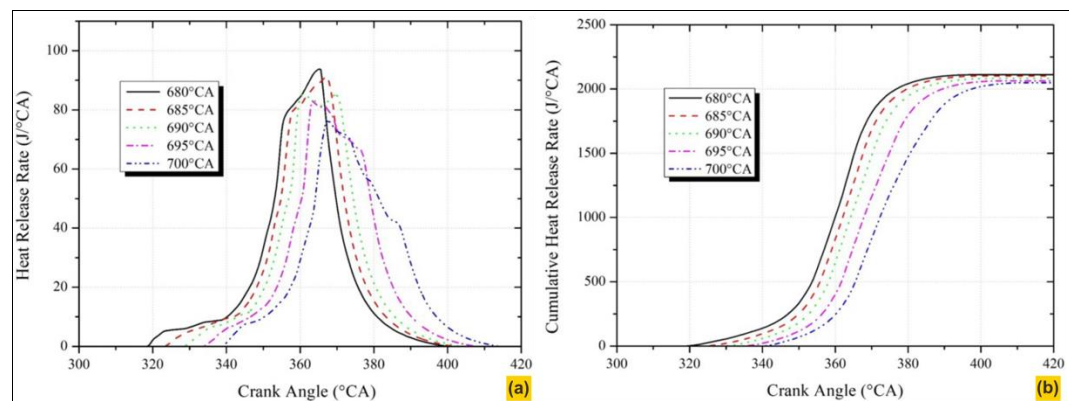
The temperature-crank angle diagrams obtained at different ignition timings of the laser ignition analysis engine are shown in **Figure 7**. The maximum in-cylinder temperature value at 680 °CA, which was determined as the optimum ignition timing for laser ignition, was lower than the 685, 690, and 695 °CA ignition timings. At this ignition timing, where maximum power, torque, work, and in-cylinder pressure occur, relatively low in-cylinder temperatures positively affect exhaust emissions. The lower in-

cylinder temperature value resulting in laser ignition with appropriate ignition advance is effective in reducing NOx emissions [90].

#### 4.7. HRR and CHRR

The HRR diagrams obtained at different ignition timings of the laser ignition analysis engine are shown in Figure 8a. Similarly, HRR got the highest value at 680 °CA ignition timing. When the HRR diagrams are examined in detail, the importance of the piston position at the crank angle, where the maximum pressure and temperature occurs, becomes stronger. In 680, 685, and 690 °CA ignition timings, the amount of positive work acting on the piston increases with the ignition in the appropriate position and the maximum pressure formation. At 695 and 700 °CA ignition timings, the combustion process passes into the expansion stroke, reducing the positive work. The increments and forms of HRR for different ignition timings also confirm this. The CHRR diagrams obtained at different ignition timings of the laser ignition analysis engine are shown in Figure 8b. A decrease was observed in the amount of CHRR with the decreasing amount of ignition advance.

**Figure 8.**  
(a) HRR-crank angle diagrams for laser ignition timings;  
(b) CHRR-crank angle diagrams for laser ignition timings



### 5. Conclusion

This numerical study aims to analyze the laser ignition system with a dynamic CFD model, including the entire engine cycle. The effects of spark and laser ignition systems on engine performance at different ignition timings on the internal combustion engine model are analyzed comparatively. As a result of the analysis, power, torque, IMEP, MPRR, peak pressure, start of combustion, and combustion duration values, which are critical for engine and combustion performance, were compared for both ignition systems. Pressure, temperature, and volume changes, as well as HRR and CHRR diagrams, were obtained for the laser ignition engine. The following findings were obtained from the study.

- The laser ignition system has improved engine and combustion performance for all ignition timings.
- The laser ignition system was beneficial in reducing the possibility of knocking.
- Power, torque and IMEP values showed that the laser ignition system offered higher performance.
- Higher MPRR and peak pressure values were obtained in the spark ignition engine. This shows that laser ignition will reduce knocking due to its smooth combustion characteristics.
- With the use of laser ignition at the appropriate ignition advance, the combustion duration is shortened.
- In the laser ignition engine, the maximum pressure value occurred at the optimum ignition timing of 680 °CA. At this ignition timing, the in-cylinder temperature value is lower than the 685, 690, and 695 °CA ignition timings.

When the results of the experimental studies are examined, the suitability of the CFD model applied in this study, the working method, the boundary conditions, and the results obtained has been proven.

### Authors' Declaration

**Authors' contributions and responsibilities** - The authors made substantial contributions to the conception and design of the study. The authors took responsibility for data analysis, interpretation, and discussion of results. The authors read and approved the final manuscript.

**Funding** – No funding information from the authors.

**Availability of data and materials** - All data is available from the authors.

**Competing interests** - The authors declare no competing interests.

**Additional information** – No additional information from the authors.

## Nomenclature

|                        |   |                          |   |
|------------------------|---|--------------------------|---|
| <b>BDC</b>             | Bottom Dead Center  | <b>P</b>                 | Pressure  |
| <b>CA</b>              | Crank Angle   | <b>P<sub>i</sub></b>     | Indicated power   |
| <b>CD</b>              | Combustion Duration   | <b>P<sub>p</sub></b>     | Piston position relative to bottom dead center  |
| <b>CFD</b>             | Computational Fluid Dynamics                                  | <b>Q</b>                 | Heat release  |
| <b>CHRR</b>            | Cumulative Heat Release Rate                                  | <b>Q<sub>c</sub></b>     | Cumulative heat release   |
| <b>HRR</b>             | Heat Release Rate   | <b>R<sub>i</sub></b>     | Net rate of production of species i by chemical reaction  |
| <b>IC</b>              | Internal Combustion   | <b>S</b>                 | Laser spot size   |
| <b>IMEP</b>            | Indicated Mean Effective Pressure                             | <b>S<sub>h</sub></b>     | Chemical reaction heat  |
| <b>LI</b>              | Laser Ignition  | <b>S<sub>i</sub></b>     | Rate of creation by addition from the dispersed phase   |
| <b>MPPRR</b>           | Maximum Pressure Rise Rate                                    | <b>S<sub>k</sub></b>     | User-defined source for k   |
| <b>SI</b>              | Spark Ignition  | <b>S<sub>ε</sub></b>     | User-defined source for ε   |
| <b>TDC</b>             | Top Dead Center   | <b>t</b>                 | Time  |
| <b>THC</b>             | Total Hydrocarbon   | <b>T</b>                 | Temperature   |
| <b>A</b>               | Empirical constant equal to 4.0                               | <b>T<sub>i</sub></b>     | Indicated torque  |
| <b>B</b>               | Empirical constant equal to 0.5                               | <b>v</b>                 | Fluid velocity vector   |
| <b>C<sub>p</sub></b>   | Heat capacity at constant pressure                            | <b>v'<sub>x,y</sub></b>  | Stoichiometric coefficient for reactant x in reaction y   |
| <b>C<sub>v</sub></b>   | Heat capacity at constant volume                              | <b>v''<sub>x,y</sub></b> | Stoichiometric coefficient for product x in reaction y  |
| <b>C<sub>3ε</sub></b>  | Model constants   | <b>V</b>                 | Volume  |
| <b>d</b>               | Laser beam diameter   | <b>V<sub>sw</sub></b>    | Swept volume  |
| <b>E</b>               | Total energy  | <b>W<sub>i</sub></b>     | Indicated work  |
| <b>f</b>               | Laser focal length  | <b>Y<sub>i</sub></b>     | Local mass fraction of species  |
| <b>g</b>               | Gravitational acceleration                                    | <b>Y<sub>M</sub></b>     | Contribution of the fluctuating dilatation in compressible turbulence to the overall dissipation rate |
| <b>G<sub>b</sub></b>   | Turbulent kinetic energies due to the buoyancy                | <b>Y<sub>P</sub></b>     | Mass fraction of any product species  |
| <b>G<sub>k</sub></b>   | Turbulent kinetic energies due to the mean velocity gradients | <b>Y<sub>R</sub></b>     | Mass fraction of a particular reactant  |
| <b>G<sub>1ε</sub></b>  | Model constants   | <b>ε</b>                 | Turbulence dissipation rate   |
| <b>G<sub>2ε</sub></b>  | Model constants   | <b>θ</b>                 | Crankshaft angular position   |
| <b>i</b>               | Number of crank revolutions for each power stroke             | <b>θ<sub>s</sub></b>     | Initial angular position of the crankshaft  |
| <b>J<sub>i</sub></b>   | Diffusion flux of species i                                   | <b>λ</b>                 | Laser wavelength  |
| <b>k</b>               | Turbulent kinetic energy                                      | <b>μ</b>                 | Viscosity   |
| <b>k<sub>eff</sub></b> | Effective thermal conductivity                                | <b>μ<sub>t</sub></b>     | Turbulent viscosity   |
| <b>L<sub>h</sub></b>   | Stroke length   | <b>ρ</b>                 | Density   |
| <b>L<sub>r</sub></b>   | Rod length  | <b>σ<sub>ε</sub></b>     | Turbulent Prandtl numbers for ε   |
| <b>M<sup>2</sup></b>   | Laser beam quality parameter                                  | <b>σ<sub>k</sub></b>     | Turbulent Prandtl numbers for k   |
| <b>M<sub>w,x</sub></b> | Molecular weight of species x                                 | <b>τ</b>                 | Internal stress forces  |
| <b>n</b>               | Engine speed  | <b>τ<sub>eff</sub></b>   | Stress tensor   |

## References

- [1] United Nations Department of Economic and Social Affairs Population Division, *World Population Prospects 2022: Summary of Results*, no. 9. 2022.
- [2] T. Kivevele, T. Raja, V. Pirouzfard, B. Waluyo, and M. Setiyo, "LPG-Fueled Vehicles: An Overview of Technology and Market Trend," *Automotive Experiences*, Apr. 2020, doi: 10.31603/ae.v3i1.3334.
- [3] S. Munahar, M. Setiyo, M. M. Saudi, A. Ahmad, and B. C. Purnomo, "Development of a transfer function (TF) model for CNG control system design predictions," *BIS Energy and Engineering*,

- vol. 1, pp. V124023–V124023, 2024, doi: 10.31603/biseeng.74.
- [4] M. H. Aditya, Y. Yuniaristanto, and W. Sutopo, "Exploring the Factors Accelerating the Electric Motorcycle Adoptions: Insights from Theory of Planned Behavior and Travel Behavior," *Automotive Experiences*, vol. 7, no. 1, pp. 171–188, May 2024, doi: 10.31603/ae.11044.
  - [5] J. E. Dakurah, H. Solmaz, and T. Kocakulak, "Modeling of a PEM Fuel Cell Electric Bus with MATLAB/Simulink," *Automotive Experiences*, vol. 7, no. 2, pp. 252–269, Sep. 2024, doi: 10.31603/ae.11471.
  - [6] S. Kaleg, D. A. Sumarsono, Y. Whulanza, and A. C. Budiman, "Addressing Fire Safety, Ground Impact Resistance, and Thermal Management in Composite EV Battery Enclosures: A Review," *Automotive Experiences*, vol. 7, no. 3, pp. 460–485, Dec. 2024, doi: 10.31603/ae.12540.
  - [7] H. Maghfiroh, O. Wahyunggoro, and A. I. Cahyadi, "Low Pass Filter as Energy Management for Hybrid Energy Storage of Electric Vehicle: A Survey," *Automotive Experiences*, vol. 6, no. 3, pp. 466–484, 2023, doi: 10.31603/ae.9398.
  - [8] H. Solmaz, T. A. Arslan, and T. Kocakulak, "Modeling of an electrically driven PEM fuel cell bus," *BIS Energy and Engineering*, vol. 1, pp. V124009–V124009, 2024, doi: 10.31603/biseeng.31.
  - [9] X. Zeng et al., "Commercialization of Lithium Battery Technologies for Electric Vehicles," *Advanced Energy Materials*, vol. 9, no. 27, Jul. 2019, doi: 10.1002/aenm.201900161.
  - [10] E. Gültekin and M. Yahşi, "Investigation of Lattice Structures for the Battery Pack Protection," *International Journal of Automotive Science and Technology*, vol. 5, no. 4, pp. 331–338, Dec. 2021, doi: 10.30939/ijastech..1020932.
  - [11] T. Alp Arslan and T. Kocakulak, "A Comprehensive Review on Stirling Engines," *Engineering Perspective*, vol. 3, no. 3, pp. 42–56, 2023, doi: 10.29228/eng.pers.66847.
  - [12] U.S. Energy Information Administration, "Short-Term Energy Outlook," *Energy Information Administration*, 2024. .
  - [13] A. Kılıç, "Charging techniques, infrastructure, and their influences," *Engineering Perspective*, vol. 3, no. 4, pp. 68–74, 2023, doi: 10.29228/eng.pers.73000.
  - [14] Straits Research, "Automotive engine market analysis, share, forecast to 2030," 2021.
  - [15] V. S. Kül and S. O. Akansu, "Experimental Investigation into the Impact of Natural Gas-Diesel Mixture on Exhaust Emissions and Engine Performance in a Heavy-Duty Diesel Engine with Six Cylinders," *International Journal of Automotive Science and Technology*, vol. 7, no. 4, pp. 360–371, Dec. 2023, doi: 10.30939/ijastech..1315920.
  - [16] H. Y. Nanlohy, S. Marianingsih, and F. Utamingrum, "A Review of the artificial neural network's roles in alternative fuels: Optimization, prediction, and future prospects," *Mechanical Engineering for Society and Industry*, vol. 4, no. 3, pp. 513–534, Dec. 2024, doi: 10.31603/mesi.12742.
  - [17] A. Sanata, I. Sholahuddin, M. D. Nashrullah, H. Y. Nanlohy, and M. S. Panithasan, "Characteristics of syngas combustion resulting from coffee husk biomass waste gasification process: Overview of automotive fuel alternatives," *Mechanical Engineering for Society and Industry*, vol. 4, no. 2, pp. 210–222, Dec. 2024, doi: 10.31603/mesi.12590.
  - [18] T. Kocakulak, T. A. Arslan, F. Şahin, H. Solmaz, S. M. S. Ardebili, and A. Calam, "Determination of optimum operating parameters of MWCNT-doped ethanol fueled HCCI engine for emission reduction," *Science of The Total Environment*, vol. 895, p. 165196, Oct. 2023, doi: 10.1016/j.scitotenv.2023.165196.
  - [19] I. Veza et al., "Strategies to achieve controlled auto-ignition (CAI) combustion: A review," *Mechanical Engineering for Society and Industry*, vol. 3, no. 1, pp. 22–34, 2023, doi: 10.31603/mesi.7568.
  - [20] W. Anggono et al., "Engine Performances of Lean Iso-Octane Mixtures in a Glow Plug Heated Sub-Chamber SI Engine," *Automotive Experiences*, vol. 5, no. 1, pp. 16–27, Nov. 2021, doi: 10.31603/ae.5118.
  - [21] A. A. Yontar and V. Wong, "Influence of laser ignition on characteristics of an engine for hydrogen enriched CNG and iso-octane usage," *International Journal of Hydrogen Energy*, vol. 46, no. 74, pp. 37071–37082, Oct. 2021, doi: 10.1016/j.ijhydene.2021.08.206.
  - [22] J. Kim, V. Gururajan, R. Scarcelli, S. Biswas, and I. Ekoto, "Modeling Nanosecond-Pulsed Spark Discharge and Flame Kernel Evolution," *Journal of Energy Resources Technology*, vol. 144, no.

- 2, Feb. 2022, doi: 10.1115/1.4051144.
- [23] H. Zang *et al.*, “Robust and ultralow-energy-threshold ignition of a lean mixture by an ultrashort-pulsed laser in the filamentation regime,” *Light: Science & Applications*, vol. 10, no. 1, p. 49, Mar. 2021, doi: 10.1038/s41377-021-00496-8.
- [24] N. Pavel, R. Chiriac, A. Birtas, F. Draghici, and M. Dinca, “On the improvement by laser ignition of the performances of a passenger car gasoline engine,” *Optics Express*, vol. 27, no. 8, p. A385, Apr. 2019, doi: 10.1364/OE.27.00A385.
- [25] T. Kocakulak *et al.*, “A new nanocomposite membrane based on sulfonated polysulfone boron nitride for proton exchange membrane fuel cells: Its fabrication and characterization,” *Fuel*, vol. 374, p. 132476, Oct. 2024, doi: 10.1016/j.fuel.2024.132476.
- [26] J. V. Pastor, J. M. García-Oliver, A. García, and M. Pinotti, “Effect of laser induced plasma ignition timing and location on Diesel spray combustion,” *Energy Conversion and Management*, vol. 133, pp. 41–55, Feb. 2017, doi: 10.1016/j.enconman.2016.11.054.
- [27] A. P. Singh, D. Kumar, and A. K. Agarwal, “Particulate characteristics of laser ignited hydrogen enriched compressed natural gas engine,” *International Journal of Hydrogen Energy*, vol. 45, no. 35, pp. 18021–18031, Jul. 2020, doi: 10.1016/j.ijhydene.2020.05.005.
- [28] D. K. Srivastava and A. K. Agarwal, “Comparative experimental evaluation of performance, combustion and emissions of laser ignition with conventional spark plug in a compressed natural gas fuelled single cylinder engine,” *Fuel*, vol. 123, pp. 113–122, May 2014, doi: 10.1016/j.fuel.2014.01.046.
- [29] C. Xu, D. Fang, Q. Luo, J. Ma, and Y. Xie, “A comparative study of laser ignition and spark ignition with gasoline–air mixtures,” *Optics & Laser Technology*, vol. 64, pp. 343–351, Dec. 2014, doi: 10.1016/j.optlastec.2014.05.009.
- [30] T. X. Phuoc, “Laser-induced spark ignition fundamental and applications,” *Optics and Lasers in Engineering*, vol. 44, no. 5, pp. 351–397, May 2006, doi: 10.1016/j.optlaseng.2005.03.008.
- [31] M. Weinrotter, H. Kopecek, M. Tesch, E. Wintner, M. Lackner, and F. Winter, “Laser ignition of ultra-lean methane/hydrogen/air mixtures at high temperature and pressure,” *Experimental Thermal and Fluid Science*, vol. 29, no. 5, pp. 569–577, Jun. 2005, doi: 10.1016/j.expthermflusci.2004.08.002.
- [32] D. R. Lancaster, R. B. Krieger, S. C. Sorenson, and W. L. Hull, “Effects of Turbulence on Spark-Ignition Engine Combustion,” Feb. 1976, doi: 10.4271/760160.
- [33] M. H. Morsy, “Review and recent developments of laser ignition for internal combustion engines applications,” *Renewable and Sustainable Energy Reviews*, vol. 16, no. 7, pp. 4849–4875, Sep. 2012, doi: 10.1016/j.rser.2012.04.038.
- [34] J. Graf, M. Weinrotter, H. Kopecek, and E. Wintner, “Laser Ignition, Optics and Contamination of Optics in an I.C. Engine,” in *ASME 2004 Internal Combustion Engine Division Fall Technical Conference*, Jan. 2004, pp. 11–17, doi: 10.1115/ICEF2004-0833.
- [35] D. Srivastava and A. K. Agarwal, “Laser Ignition of Single Cylinder Engine and Effects of Ignition Location,” Apr. 2013, doi: 10.4271/2013-01-1631.
- [36] C. Xu, D. Fang, Q. Luo, J. Ma, Y. Xie, and X. Zheng, “Characterization of gasoline combustion with laser and spark ignition,” *Journal of Zhejiang University-SCIENCE A*, vol. 16, no. 10, pp. 830–838, Oct. 2015, doi: 10.1631/jzus.A1500039.
- [37] I. A. Mulla, S. R. Chakravarthy, N. Swaminathan, and R. Balachandran, “Evolution of flame-kernel in laser-induced spark ignited mixtures: A parametric study,” *Combustion and Flame*, vol. 164, pp. 303–318, Feb. 2016, doi: 10.1016/j.combustflame.2015.11.029.
- [38] M. Cordier, A. Vandel, G. Cabot, B. Renou, and A. M. Boukhalfa, “Laser-Induced Spark Ignition of Premixed Confined Swirled Flames,” *Combustion Science and Technology*, vol. 185, no. 3, pp. 379–407, Mar. 2013, doi: 10.1080/00102202.2012.725791.
- [39] D. K. Srivastava, E. Wintner, and A. K. Agarwal, “Effect of focal size on the laser ignition of compressed natural gas–air mixture,” *Optics and Lasers in Engineering*, vol. 58, pp. 67–79, Jul. 2014, doi: 10.1016/j.optlaseng.2014.01.023.
- [40] H. Cheng, V. Page, Z. Kuang, E. Lyon, G. Dearden, and T. Shenton, “Multiple Pulse Laser Ignition Control Application in GDI Lean Combustion,” in *Laser Ignition Conference*, 2015, p. W2A.2, doi: 10.1364/LIC.2015.W2A.2.
- [41] P. Patane and M. Nandgaonkar, “Review: Multipoint laser ignition system and its applications to IC engines,” *Optics & Laser Technology*, vol. 130, p. 106305, Oct. 2020, doi:

- 10.1016/j.optlastec.2020.106305.
- [42] R. K. Prasad and A. K. Agarwal, "Effect of hydrogen enrichment of compressed natural gas on combustible limit and flame kernel evolution in a constant volume combustion chamber using laser ignition," *Fuel*, vol. 302, p. 121112, Oct. 2021, doi: 10.1016/j.fuel.2021.121112.
- [43] R. K. Prasad and A. K. Agarwal, "Experimental evaluation of laser ignited hydrogen enriched compressed natural gas fueled supercharged engine," *Fuel*, vol. 289, p. 119788, Apr. 2021, doi: 10.1016/j.fuel.2020.119788.
- [44] L. Schroeder, T. Hillenbrand, and D. Brueggemann, "Comparison of a Laser Ignition with an Electrical Spark Ignitions System for Directly Injected Methane in a Rapid Compression Machine," Aug. 2022, doi: 10.4271/2022-01-1062.
- [45] H. Zang et al., "Goldilocks focal zone in femtosecond laser ignition of lean fuels," *Science China Technological Sciences*, vol. 65, no. 7, pp. 1537–1544, Jul. 2022, doi: 10.1007/s11431-022-2049-1.
- [46] N. Pothanna and P. Aparna, "Unsteady thermoviscous flow in a porous slab over an oscillating flat plate," *Journal of Porous Media*, vol. 22, no. 5, pp. 531–543, 2019, doi: 10.1615/JPorMedia.2019028871.
- [47] N. Pothanna, P. Aparna, and J. Srinivas, "Unsteady Forced Oscillations of a Fluid Bounded by Rigid Bottom," *International Journal of Control Theory and Applications*, vol. 9, no. 19, pp. 9049–9054, 2016.
- [48] A. Ikpe and M. Bassey, "Computational Fluid Dynamics of Four Stroke In-Cylinder Charge Behavior at Distinct Valve Lift Opening Clearance in Spark Ignition Reciprocating Internal Combustion Renault Engine," *International Journal of Automotive Science and Technology*, vol. 8, no. 1, pp. 1–22, Mar. 2024, doi: 10.30939/ijastech..1337386.
- [49] E. Arabacı, Ş. Öztürü, and S. Halis, "Simulation of The Effects of Valve Timing Misalignment on Performance in Spark Ignition Engines," *Engineering Perspective*, vol. 4, no. 2, pp. 47–53, 2024, doi: 10.29228/eng.pers.75927.
- [50] S. A. Basha and K. Raja Gopal, "In-cylinder fluid flow, turbulence and spray models—A review," *Renewable and Sustainable Energy Reviews*, vol. 13, no. 6–7, pp. 1620–1627, Aug. 2009, doi: 10.1016/j.rser.2008.09.023.
- [51] M. Firat and Y. Varol, "A Comparative Analysis of In-Cylinder Flow, Heat Transfer and Turbulence Characteristics in Different Type Combustion Chamber," *International Journal of Automotive Engineering and Technologies*, vol. 7, no. 1, pp. 18–28, Apr. 2018, doi: 10.18245/ijaet.438043.
- [52] O. Moussa, A. Ketata, D. Zied, and P. Coelho, "In-Cylinder Aero-Thermal Simulation of Compression Ignition Engine: Using a Layering Meshing Approach," *Journal of Applied Fluid Mechanics*, vol. 12, no. 5, pp. 1651–1665, Sep. 2019, doi: 10.29252/jafm.12.05.29536.
- [53] S. D. Zambalov, I. A. Yakovlev, and V. A. Skripnyak, "Numerical simulation of hydrogen combustion process in rotary engine with laser ignition system," *International Journal of Hydrogen Energy*, vol. 42, no. 27, pp. 17251–17259, Jul. 2017, doi: 10.1016/j.ijhydene.2017.05.142.
- [54] P. M. Patane and M. R. Nandgaonkar, "Numerical simulation of combustion characteristics and emission predictions of methane-air and hydrogen-air mixtures in a constant volume combustion chamber using multi-point laser-induced spark ignition," *Energy Sources, Part A: Recovery, Utilization, and Environmental Effects*, pp. 1–17, Apr. 2021, doi: 10.1080/15567036.2021.1910383.
- [55] S. S. Patil and M. R. Nandgaonkar, "Numerical analysis of gasoline fuel with laser ignited spark ignition," *Journal of Physics: Conference Series*, vol. 1240, no. 1, p. 012037, Jul. 2019, doi: 10.1088/1742-6596/1240/1/012037.
- [56] T. X. Phuoc, "An experimental and numerical study of laser-induced spark in air," *Optics and Lasers in Engineering*, vol. 43, no. 2, pp. 113–129, Feb. 2005, doi: 10.1016/j.optlaseng.2004.07.003.
- [57] D. Kumar and A. K. Agarwal, "Laser ignition versus conventional spark ignition system performance for hydrogen-enriched natural gas-air mixtures in a constant volume combustion chamber," *Applied Thermal Engineering*, vol. 257, p. 123988, Dec. 2024, doi: 10.1016/j.applthermaleng.2024.123988.
- [58] A. K. Agarwal, A. P. Singh, and A. Pal, "Effect of laser parameters and compression ratio on

- particulate emissions from a laser ignited hydrogen engine," *International Journal of Hydrogen Energy*, vol. 42, no. 15, pp. 10622–10635, Apr. 2017, doi: 10.1016/j.ijhydene.2017.03.074.
- [59] S. Azarmanesh and M. Z. Targhi, "Comparison of laser ignition and spark plug by thermodynamic simulation of multi-zone combustion for lean methane-air mixtures in the internal combustion engine," *Energy*, vol. 216, p. 119309, Feb. 2021, doi: 10.1016/j.energy.2020.119309.
- [60] T.-T. Do, L. V. Dat, and T.-N. Dinh, "Motorcycle Engine Performance Comparison Between Laser Ignition System and Conventional Ignition System Through Simulation," *International Journal of Automotive and Mechanical Engineering*, vol. 21, no. 2, pp. 11332–11349, Jun. 2024, doi: 10.15282/ijame.21.2.2024.12.0875.
- [61] N. Bhondwe and C. D. Koshti, "International Engineering Research Journal CFD Analysis of Premixed Methane-Air Combustion using Laser Ignition," *International Engineering Research Journal*, vol. Special Ed, pp. 1–5, 2017, doi: 10.13140/RG.2.2.14760.39682.
- [62] T. A. Arslan, H. Bayrakçeken, and H. Yavuz, "CFD Analysis of Sloshing in the Fuel Tank of a Heavy Vehicle with Emergency Braking System," *International Journal of Automotive Science and Technology*, vol. 7, no. 4, pp. 340–348, Dec. 2023, doi: 10.30939/ijastech..1360466.
- [63] N. Pothanna, P. Aparna, and R. S. R. Gorla, "A Numerical Study of Coupled Non-Linear Equations of Thermo-Viscous Fluid Flow in Cylindrical Geometry," *International Journal of Applied Mechanics and Engineering*, vol. 22, no. 4, pp. 965–979, Dec. 2017, doi: 10.1515/ijame-2017-0062.
- [64] T. M. Belal, E. S. M. Marzouk, and M. M. Osman, "Investigating Diesel Engine Performance and Emissions Using CFD," *Energy and Power Engineering*, vol. 05, no. 02, pp. 171–180, 2013, doi: 10.4236/epe.2013.52017.
- [65] T. Endo, K. Kuwamoto, W. Kim, T. Johzaki, D. Shimokuri, and S. Namba, "Comparative study of laser ignition and spark-plug ignition in high-speed flows," *Combustion and Flame*, vol. 191, pp. 408–416, May 2018, doi: 10.1016/j.combustflame.2018.01.029.
- [66] D. H. McNeill, "Minimum ignition energy for laser spark ignition," *Proceedings of the Combustion Institute*, vol. 30, no. 2, pp. 2913–2920, Jan. 2005, doi: 10.1016/j.proci.2004.07.026.
- [67] T. Badawy, X. Bao, and H. Xu, "Impact of spark plug gap on flame kernel propagation and engine performance," *Applied Energy*, vol. 191, pp. 311–327, Apr. 2017, doi: 10.1016/j.apenergy.2017.01.059.
- [68] Y. V. Anishchanka, E. Y. Loktionov, and V. D. Telekh, "Investigation of minimum laser ignition energies of combustible gas mixtures," *Journal of Physics: Conference Series*, vol. 1115, p. 042020, Nov. 2018, doi: 10.1088/1742-6596/1115/4/042020.
- [69] M. Weinrotter, H. Kopecek, E. Wintner, M. Lackner, and F. Winter, "Application of laser ignition to hydrogen-air mixtures at high pressures," *International Journal of Hydrogen Energy*, vol. 30, no. 3, pp. 319–326, Mar. 2005, doi: 10.1016/j.ijhydene.2004.03.040.
- [70] R. Dodd *et al.*, "Laser ignition of an IC test engine using an Nd: YAG laser and the effect of key laser parameters on engine combustion performance," *Lasers in Engineering*, vol. 17, no. 3–4, pp. 213–231, 2007.
- [71] W. Wang, Y. Cao, and T. Okaze, "Comparison of hexahedral, tetrahedral and polyhedral cells for reproducing the wind field around an isolated building by LES," *Building and Environment*, vol. 195, p. 107717, May 2021, doi: 10.1016/j.buildenv.2021.107717.
- [72] T. A. Arslan, H. Solmaz, D. İpci, and F. Aksoy, "Investigation of the effect of compression ratio on performance of a beta type Stirling engine with rhombic mechanism by <sc>CFD</sc> analysis," *Environmental Progress & Sustainable Energy*, vol. 42, no. 4, Jul. 2023, doi: 10.1002/ep.14076.
- [73] W. Zhao, R. Li, H. Li, Y. Zhang, and S. Qiu, "Numerical analysis of fluid dynamics and thermodynamics in a stirling engine," *Applied Thermal Engineering*, vol. 189, p. 116727, May 2021, doi: 10.1016/j.applthermaleng.2021.116727.
- [74] F. Perini *et al.*, "Piston geometry effects in a light-duty, swirl-supported diesel engine: Flow structure characterization," *International Journal of Engine Research*, vol. 19, no. 10, pp. 1079–1098, Dec. 2018, doi: 10.1177/1468087417742572.
- [75] R. Ortiz-Imedio, A. Ortiz, and I. Ortiz, "Comprehensive analysis of the combustion of low

- carbon fuels (hydrogen, methane and coke oven gas) in a spark ignition engine through CFD modeling,” *Energy Conversion and Management*, vol. 251, p. 114918, Jan. 2022, doi: 10.1016/j.enconman.2021.114918.
- [76] T. A. Arslan, H. Solmaz, and D. İpci, “Rhombic Mekanizmalı Beta Tipi Bir Stirling Motorunun Adyabatik Şartlarda CFD Analizi,” 2021.
- [77] X. Luo, X. Yu, K. Zha, M. Jansons, and V. Soloiu, “In-Cylinder Wall Temperature Influence on Unburned Hydrocarbon Emissions During Transitional Period in an Optical Engine Using a Laser-Induced Phosphorescence Technique,” *SAE International Journal of Engines*, vol. 7, no. 2, pp. 2014-01–1373, Apr. 2014, doi: 10.4271/2014-01-1373.
- [78] J. Zhang, Z. Xu, J. Lin, Z. Lin, J. Wang, and T. Xu, “Thermal Characteristics Investigation of the Internal Combustion Engine Cooling-Combustion System Using Thermal Boundary Dynamic Coupling Method and Experimental Verification,” *Energies*, vol. 11, no. 8, p. 2127, Aug. 2018, doi: 10.3390/en11082127.
- [79] H. Heisler, *Vehicle and Engine Technology*, 2nd ed. Society of Automotive Engineers, 1999.
- [80] E. Surer, H. Solmaz, E. Yılmaz, A. Calam, and D. İpci, “Dizel-biyodizel karışımına karbon nanotüp katkısının motor performansı ve egzoz emisyonlarına etkisinin incelenmesi,” *Gazi Üniversitesi Mühendislik Mimarlık Fakültesi Dergisi*, vol. 38, no. 2, pp. 1055–1064, Oct. 2022, doi: 10.17341/gazimmfd.741177.
- [81] S. Polat, A. Calam, S. Ardebili, F. Şahin, A. Boroïu, and H. Solmaz, “Operating Range, Performance and Emissions of an HCCI Engine Fueled with Fusel Oil/Diethyl Ether: An Experimental Study,” *Sustainability*, vol. 14, no. 23, p. 15666, Nov. 2022, doi: 10.3390/su142315666.
- [82] H. Solmaz, A. Calam, S. Halis, D. İpci, and E. Yılmaz, “HCCI bir motorda emme manifoldu basıncının performans ve yanma karakteristiklerine etkilerinin incelenmesi,” *Gazi Üniversitesi Mühendislik Mimarlık Fakültesi Dergisi*, vol. 37, no. 4, pp. 1735–1750, Feb. 2022, doi: 10.17341/gazimmfd.602742.
- [83] P. T. Kale, “Combustion of biodiesel in CI engine,” *International Journal of Applied Research*, vol. 3, no. 3, pp. 145–149, 2017.
- [84] İ. Örs, M. Ciniviz, and B. S. Kul, “Comparison of Performance , Emission and Combustion Characteristics of Waste Frying Oil Biodiesel with Cotton Oil and Safflower Oil Biodiesels Atık Kızartma Yağı Biyodizelinin Performans , Emisyon ve Yanma Karakteristiklerinin Pamuk Yağı ve Aspir Yağı Biy,” *Journal of Institute Of Science and Technology*, vol. 37, no. 3, 2021.
- [85] Y. Sekmen, P. Sekmen, and M. Salman, “The effect of compression ratio on engine performance and exhaust emission in a spark ignition engine,” *Journal of the Faculty of Engineering and Architecture of Gazi University*, vol. 22, pp. 745–751, Dec. 2007.
- [86] A. Calam, Y. İçingür, and S. Halis, “HCCI Bir Motorda Oktan Sayısının Yanma Karakteristiklerine Etkisi,” 2018.
- [87] C. Zhang, A. Zhou, Y. Shen, Y. Li, and Q. Shi, “Effects of combustion duration characteristic on the brake thermal efficiency and NOx emission of a turbocharged diesel engine fueled with diesel-LNG dual-fuel,” *Applied Thermal Engineering*, vol. 127, pp. 312–318, Dec. 2017, doi: 10.1016/j.applthermaleng.2017.08.034.
- [88] N. Pavel et al., “Laser ignition - Spark plug development and application in reciprocating engines,” *Progress in Quantum Electronics*, vol. 58, pp. 1–32, Mar. 2018, doi: 10.1016/j.pquantelec.2018.04.001.
- [89] A. Birtas, G. Croitoru, M. Dinca, T. Dascalu, N. Boicea, and N. Pavel, “The effect of laser ignition on a homogenous lean mixture of an automotive gasoline engine,” 2016.
- [90] V. Ayhan, “Direk Enjeksiyonlu Bir Dizel Motoruna Buhar ve Farklı Şekillerde Su Gönderiminin Performans ve NOx Emisyonlarına Etkilerinin İncelenmesi,” *SAÜ Fen Bilimleri Enstitüsü Dergisi*, vol. 20, no. 3, Sep. 2016, doi: 10.16984/saufenbilder.91773.